

# NJC

Accepted Manuscript



This is an *Accepted Manuscript*, which has been through the Royal Society of Chemistry peer review process and has been accepted for publication.

*Accepted Manuscripts* are published online shortly after acceptance, before technical editing, formatting and proof reading. Using this free service, authors can make their results available to the community, in citable form, before we publish the edited article. We will replace this *Accepted Manuscript* with the edited and formatted *Advance Article* as soon as it is available.

You can find more information about *Accepted Manuscripts* in the [Information for Authors](#).

Please note that technical editing may introduce minor changes to the text and/or graphics, which may alter content. The journal's standard [Terms & Conditions](#) and the [Ethical guidelines](#) still apply. In no event shall the Royal Society of Chemistry be held responsible for any errors or omissions in this *Accepted Manuscript* or any consequences arising from the use of any information it contains.

# Tuning the Topology Structures of Polymolybdate-based Hybrids from Interpenetrated Framework to Interdigitated Architecture *via* Changing Polymolybdate Clusters†

Shaobin Li, Li Zhang, Huiyuan Ma\*, Haijun Pang\* and Chunyan Zhao

*Key Laboratory of Green Chemical Engineering and Technology of College of Heilongjiang Province, College of Chemical and Environmental Engineering, Harbin University of Science and Technology, Harbin 150040, China Tel.: 86-0451-86392716, Fax: 86-0451-86392716; E-mail: mahy017@163.com (Ma H. Y.), panghj116@163.com (Pang. H. J.).*

†Electronic supplementary information (ESI) available: Additional figures, IR, and PXRD. See DOI:

By introducing different polyoxomolybdates into the Cu-bimb system (bimb = 1,4-bis(imidazol-1-yl) benzene), three new polyoxomolybdate-based inorganic-organic hybrids with distinct architectures,  $[\text{Cu}^{\text{II}}(\text{bimb})_{1.5}(\text{H}_2\text{O})(\beta\text{-Mo}_8\text{O}_{26})_{0.5}]$  (**1**),  $(\text{Hbimb})_2[\text{Cu}^{\text{I}}(\text{bimb})(\text{PMo}_{12}\text{O}_{40})]\cdot 4\text{H}_2\text{O}$  (**2**) and  $[\text{Cu}^{\text{I}}_4(\text{bimb})_4(\text{SiMo}_{12}\text{O}_{40})]\cdot 2\text{H}_2\text{O}$  (**3**), have been synthesized under identical hydrothermal conditions and characterized by routine methods. Compound **1** displays an interesting 2-fold interpenetrated structure constructed by two identical layers. When the polyoxomolybdate clusters were changed from  $\beta\text{-}[\text{Mo}_8\text{O}_{26}]^{4-}$  to  $[\text{PMo}_{12}\text{O}_{40}]^{3-}$ , and  $[\text{SiMo}_{12}\text{O}_{40}]^{4-}$ , compounds **2** and **3** were obtained, respectively. Compound **2** shows a highly opened three-dimensional framework while compound **3** exhibits a three-dimensional interdigitated architecture. The different structural features of compounds **1–3** suggest that the influence of different polyoxometalate clusters on structures should play a key role in the process of assembling. Additionally, both the luminescent and electrochemical properties for **1–3** have been

investigated.

## Introduction

As a new generation of solid-state materials,<sup>1a</sup> the inorganic-organic hybrids constructed from metal ions as connectors and ligands as linkers have attracted increasing attention, owing to their enormous varieties of interesting structural topologies and wide potential applications in several fields, such as molecular recognition, catalysis, absorption, and photosensitive materials.<sup>1,2</sup>

Polyoxometalates (POMs), as inorganic building blocks, have a large number of surface oxygen atoms, which make them possess abundant potential active coordination sites and show versatile coordination modes. Also, the POMs exhibit the superior potential applications especially in catalysis and electrochemistry.<sup>3</sup> In virtue of their special properties a promising route is the use of the POMs as secondary building units (SBUs) to construct POM-based inorganic-organic hybrids. This method incorporates two important fields of both POMs and common inorganic-organic hybrid materials and opens up new possibilities in pursuit of multifunctional materials.<sup>4</sup>

The hydrothermal synthesis method is well known as a powerful technique for the preparation of the POM-based inorganic-organic hybrids. Generally, the hybrids prepared by hydrothermal reaction are poor solubility in water and in common inorganic and/or organic solvent. This property is very advantageous to expand applications of the POM-based hybrid materials in chemically bulk-modified electrode and heterogeneous catalysis.<sup>5</sup> Nevertheless, from the crystal engineering

point of view, to realize the targeting syntheses of the resulting hybrids by hydrothermal synthesis is still a great challenge at present, because the final structures are frequently modulated by various factors. To date, thanks to the POM chemists, some pioneering works have illuminated the effect of some factors on the construction of POM-based hybrids, such as the length and flexibility of organic ligands,<sup>6</sup> the pH of reaction system, the temperature of reaction system and the nature of metal ions.<sup>7,8</sup> In our previous work, we have discussed the influence of steric hindrance of organic ligands, secondary spacers, and metal ions on the structures of POM-based hybrids.<sup>9</sup> It is well-known that POMs exhibit a wide variety of robust structural motifs of different topologies and charge.<sup>10</sup> So, the POM anion is another key factor which may influence structures of POM-based hybrids. However, the influences of POM anions on the structures of POM-based hybrid compounds have been rarely mentioned.<sup>11</sup> Thus, to further address relationships between the final structures of hybrids and the POM anions is desirable, which may provide guidance or new strategies for ongoing synthetic work.

Taking this into account, in this work, the  $\text{Mo}_8\text{O}_{26}^{4-}$  ( $\text{Mo}_8$ ) octamolybdate, the  $\text{PMo}_{12}\text{O}_{40}^{3-}$  ( $\text{PMo}_{12}$ ) and  $\text{SiMo}_{12}\text{O}_{40}^{4-}$  ( $\text{SiMo}_{12}$ ) Keggin clusters are introduced into the Cu-bimb reaction system, respectively, and three new inorganic-organic hybrids,  $[\text{Cu}^{\text{II}}(\text{bimb})_{1.5}(\text{H}_2\text{O})(\beta\text{-Mo}_8\text{O}_{26})_{0.5}]$  (**1**)  $(\text{Hbimb})_2[\text{Cu}^{\text{I}}(\text{bimb})(\text{PMo}_{12}\text{O}_{40})]\cdot 4\text{H}_2\text{O}$  (**2**) and  $[\text{Cu}^{\text{I}}_4(\text{bimb})_4(\text{SiMo}_{12}\text{O}_{40})]\cdot 2\text{H}_2\text{O}$  (**3**) have been obtained, which show distinct structure motifs from a (2D  $\rightarrow$  2D) 2-fold interpenetrated structure, a highly opened 3D framework to a (2D + 2D  $\rightarrow$  3D) interdigitated architecture, which shows that the

influence of different polymolybdates is a key factor to control the structures of the hybrid compounds. Furthermore, the luminescent and electrochemical properties for **1–3** have been investigated in details.

## Experimental Section

### Materials and General Methods

All reagents were purchased commercially and were used without further purification. Elemental analyses (C, H and N) were performed on a Perkin-Elmer 2400 CHN Elemental Analyzer. Elemental Analyzer and that of Cu and W were carried out with a Leaman inductively coupled plasma (ICP) spectrometer. The FT-IR spectra were recorded from KBr pellets in the range 4000–400  $\text{cm}^{-1}$  with a Nicolet AVATAR FT-IR360 spectrometer. A CHI660 electrochemical workstation was used for control of the electrochemical measurements and data collection. A conventional three-electrode system was used, with a carbon paste electrode (CPE) as a working electrode, a commercial Ag/AgCl as reference electrode and a twisted platinum wire as counter electrode. The powder X-ray diffraction (PXRD) data were collected on a Rigaku RINT2000 diffractometer at room temperature.

### Preparations

#### $[\text{Cu}^{\text{II}}(\text{bimb})_{1.5}(\text{H}_2\text{O})(\beta\text{-Mo}_8\text{O}_{26})_{0.5}]$ (**1**)

A mixture of  $(\text{NH}_4)_6\text{Mo}_7\text{O}_{24}\cdot 4\text{H}_2\text{O}$  (0.37 g, 0.3mmol),  $\text{CuCl}_2\cdot 2\text{H}_2\text{O}$  (0.16 g, 0.9 mmol), bimb (0.08 g, 0.38 mmol) and water (10 mL) was stirred for 1h. The resulting solution was transferred to a Teflon lined autoclave and kept under autogenous

pressure at 160 °C for 4 days with a starting pH = 3.3–3.8 adjusted by 3 M HCl. After slow cooling to room temperature, blue block crystals of **1** were filtered, washed with distilled water and dried at room temperature (Yield, 48 %, based on Mo). Anal. Calcd for C<sub>18</sub>H<sub>17</sub>CuMo<sub>4</sub>N<sub>6</sub>O<sub>14</sub>: C 21.87, H 1.73, N 8.50, Cu 6.43, Mo 38.82 %; Found: C 21.99, H 1.61, N 8.39, Cu 6.23, Mo 38.99 %.

**(Hbimb)<sub>2</sub>[Cu<sup>I</sup>(bimb)(PMo<sub>12</sub>O<sub>40</sub>)]·4H<sub>2</sub>O (2)**

The synthetic method was similar to that of compound **1**, except that the (NH<sub>4</sub>)<sub>6</sub>Mo<sub>7</sub>O<sub>24</sub>·4H<sub>2</sub>O was replaced by H<sub>3</sub>PMo<sub>12</sub>O<sub>40</sub>. Dark brown block crystals of **2** were filtered, washed with water, and dried at room temperature. Yield: 45 % (based on Mo). Anal. calcd. for C<sub>36</sub>H<sub>40</sub>CuMo<sub>12</sub>N<sub>12</sub>O<sub>44</sub>P: C 16.69, H 1.56, N 6.49, Cu 2.45, Mo 44.44%; Found: C 16.58, H 1.64, N 6.39, Cu 2.32, Mo 44.58 %.

**[Cu<sup>I</sup><sub>4</sub>(bimb)<sub>4</sub>(SiMo<sub>12</sub>O<sub>40</sub>)]·2H<sub>2</sub>O (3)**

The synthetic method was similar to that of compound **1**, except that the (NH<sub>4</sub>)<sub>6</sub>Mo<sub>7</sub>O<sub>24</sub>·4H<sub>2</sub>O was replaced by H<sub>4</sub>SiMo<sub>12</sub>O<sub>40</sub>. Dark brown block crystals of **3** were filtered, washed with distilled water and dried at room temperature (Yield, 43 %, based on Mo). Anal. Calcd for C<sub>48</sub>H<sub>44</sub>Cu<sub>4</sub>Mo<sub>12</sub>N<sub>16</sub>O<sub>42</sub>Si: C 19.54, H 1.50, N 7.60, Cu 8.61, Mo 39.02 %; Found: C 19.64, H 1.59, N 7.49, Cu 8.79, Mo 38.81 %.

**Preparation of 1-, 2- and 3-CPEs:** the compound **1** modified carbon paste electrodes (**1-CPE**) was fabricated as follows: 60 mg of graphite powder and 9 mg of compound **1** were mixed and ground together by agate mortar and pestle to achieve a uniform mixture, and then 0.6 mL of nujol was added with stirring. The homogenized mixture was packed into a glass tube with a 1.2 mm inner diameter, and the tube surface was

wiped with paper. Electrical contact was established with a copper rod through the back of the electrode. In a similar manner, the **2**- and **3**-CPEs were made with compounds **2** and **3**, respectively.

### X-ray Crystallographic Study

Single-crystal X-ray diffraction data collections of **1–3** were performed using a Bruker Smart Apex CCD diffractometer with Mo-K $\alpha$  radiation ( $\lambda = 0.71073 \text{ \AA}$ ) at 293 K. Multi-scan absorption corrections were applied.<sup>12</sup> The structure was solved by Direct Methods and refined by full-matrix least-squares on  $F^2$  using the SHELXTL 97 crystallographic software package.<sup>13</sup> Anisotropic displacement parameters were used to refine all non-hydrogen atoms. The organic hydrogen atoms were generated geometrically. All H atoms on C and N atoms were fixed at the calculated positions. The H atoms on water molecules in **2** were fixed at the calculated positions, while the H atoms on water molecules in **1** and **3** can not be found from the residual peaks and were directly included in the final molecular formula. A summary of the crystal data, data collections and refinement parameters for **1–3** are listed in Table 1. Crystallographic data for the structures reported in this paper have been deposited in the Cambridge Crystallographic Data Center with CCDC Number: 1014808 for **1**, 1014809 for **2** and 1014810 for **3**.

**Table 1** Crystal data and structure refinement for **1–3**.

	<b>1</b>	<b>2</b>	<b>3</b>
Empirical formula	C <sub>18</sub> H <sub>17</sub> CuMo <sub>4</sub> N <sub>6</sub> O <sub>14</sub>	C <sub>36</sub> H <sub>40</sub> CuMo <sub>12</sub> N <sub>12</sub> O <sub>44</sub> P	C <sub>48</sub> H <sub>44</sub> Cu <sub>4</sub> Mo <sub>12</sub> N <sub>16</sub> O <sub>42</sub> Si
<i>Mr</i>	988.67	2590.58	2950.53
Crystal system	Monoclinic	Triclinic	Triclinic
Space group	<i>P</i> 2 <sub>1</sub> / <i>c</i>	<i>P</i> $\bar{1}$	<i>P</i> $\bar{1}$
<i>a</i> , $\text{\AA}$	10.6473(19)	11.158(5)	10.9784(9)
<i>b</i> , $\text{\AA}$	19.752(4)	12.946(5)	14.0480(11)

$c$ , Å	13.4070(16)	13.292(5)	14.5469(12)
$\alpha$ , deg	90	97.478(5)	110.234(2)
$\beta$ , deg	113.396(10)	112.381(5)	107.408(1)
$\gamma$ , deg	90	104.018(5)	102.658(1)
$V$ , Å <sup>3</sup>	2587.8(8)	1668.8(12)	1873.7(3)
$Z$	4	1	1
$D_{\text{calcd}}$ , g cm <sup>-3</sup>	2.533	2.574	2.611
Temperature K	293(2)	293(2)	293(2)
Absorption coeff. ( $\mu$ ) mm <sup>-1</sup>	2.777	2.618	3.164
$\theta_{\text{max}}$ , $\theta_{\text{min}}$ (°)	25.07, 1.95	25.24, 1.67	25.14, 1.64
$F(000)$	1896.0	1236.0	1410.0
Independent reflections	4599 [ $R(\text{int}) = 0.0835$ ]	6050 [ $R(\text{int}) = 0.0331$ ]	6693 [ $R(\text{int}) = 0.0302$ ]
Goodness-of-fit on $F^2$	1.030	1.024	1.041
$^a R_1 / ^b wR_2$ [ $I \geq 2\sigma(I)$ ]	0.0553/ 0.0995	0.0716/ 0.1931	0.0534/ 0.0944
Largest diff. Peak and hole e Å <sup>-3</sup>	1.152 and -0.799	2.450 and -1.504	1.202 and -0.965

$$^a R_1 = \frac{\sum \|F_o\| - \|F_c\|}{\sum \|F_o\|}, \quad ^b wR_2 = \frac{\sum [w(F_o^2 - F_c^2)^2]}{\sum [w(F_o^2)^2]}^{1/2}$$

## Results and discussion

Hydrothermal synthesis has recently been proved to be a powerful method in the synthesis of POM-based hybrid compounds. Many factors can affect the produce of final products during a specific hydrothermal synthesis, such as the starting concentrations of reactants, time, pH values, mineralization and temperature. In our case, parallel experiments show that the pH values of the reaction system are crucial for the formation of the compounds. Compound **1** could only be obtained at pH value of 2.5, and compounds **2** and **3** could be obtained at pH values of 3–4. When the pH value was lower or higher than that specific value, the expected crystals could not be obtained. The networks of compounds **1–3** were analyzed by using the Olex program.<sup>14</sup>

## Description of the Crystal Structure

### Crystal Structure of compound **1**

X-ray crystal structure analysis reveals that compound **1** consists of one crystallographically Cu(II) ion, one and a half bimb ligands, and half a  $[\beta\text{-Mo}_8\text{O}_{26}]^{4-}$  anion (abbreviated as  $\text{Mo}_8$ ) (Fig. 1). The  $\text{Mo}_8$  cluster, exhibits the most compact structure of eight edge-sharing  $[\text{MoO}_6]$  octahedra with two  $[\text{Mo}_4\text{O}_{13}]$  subunits stacking together.<sup>15</sup> The  $\text{Cu}^{2+}$  cation is five-coordinated in a trigonal bipyramid coordination geometry achieved by three nitrogen atoms (N1, N2, N5) from three bimb ligands and two oxygen atoms respectively from one terminal oxygen atom (O7) of  $\text{Mo}_8$  anion and one water molecule. The bond lengths around the Cu1 atom range from 1.957(10) to 2.008(10) Å for Cu–N and from 2.118(7) to 2.138(8) Å for Cu–O. All of these bond lengths are within the normal ranges observed in other Cu(II)-containing complexes.<sup>16</sup>

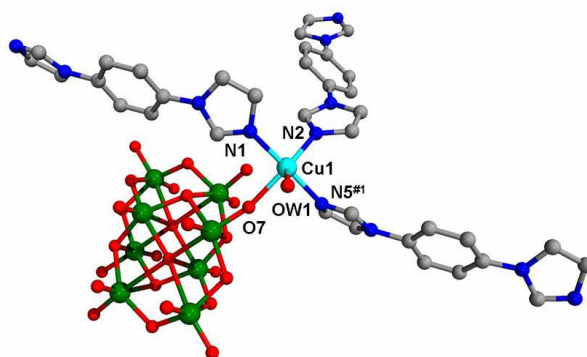


**Fig. 1** Asymmetric unit of **1** and the coordination environment of the  $\text{Cu}^{\text{II}}$  center in **1**. (All of the hydrogen atoms are omitted for clarity; Symmetry codes: #1: x, y, 1+z.)

A structural feature of **1** is a 2-fold interpenetrated ( $4^4$ ) **sql** topological structure,<sup>17</sup> which can be described in detail as follows: as shown in Fig. 2a and 2b, there is a (4, 4) undulated layer comprised of double-dentate  $\beta\text{-Mo}_8$  anions and Cu-bimb ladder-like

chains. In the undulated layer, there are two kinds of approximately rectangular cavities (A and B). The A cavity is comprised by four Cu atoms and four bimb ligands with the size of the window *ca.*  $13.407 \times 13.512 \text{ \AA}$ , while the B cavity is comprised by four Cu atoms, two bimb ligands and two  $\beta\text{-Mo}_8$  anions with the size of *ca.*  $13.407 \times 12.214 \text{ \AA}$ . As is known, large structural cavities are often occupied by solvent molecules or guest molecules to achieve the structural stabilization. Otherwise, the interpenetration phenomena may occur, that is, the cavities associated with one framework are occupied by one or more independent frameworks to fill the spaces. In **1**, the void space of the single undulated layer is so large that two identical 2D layers interpenetrate each other to form a (2D  $\rightarrow$  2D) 2-fold interpenetrated **sql** net. (Fig. 2c and 2d). In the very recently, the progress of the POM-based interpenetrated structures was well-documented in a comprehensive review organized by Su, Lan and their coworkers.<sup>18</sup> According to the reviewer's comments and the searching results of CSD database, there are five examples of POM-based compounds showing the (2D  $\rightarrow$  2D) 2-fold interpenetration structures have been reported till now, and all of them are constructed from the flexible multidentate ligands btx and ttb.<sup>19</sup> Compared to five examples, compound **1** represents an exceptional POM-based 2-fold interpenetrated case assembled from the rigid ligand bimb. Furthermore, after detailed view of the structure compound **1**, there exist two kinds of interpenetrating motifs (A and B). The motif A is composed of two different structural fragments: Cu-bimb-Mo<sub>8</sub> ladder and Cu-bimb ladder (Fig. 3a), while, the motif B is composed of identical structural fragments: two Cu-bimb-Mo<sub>8</sub> ladders (Fig. 3b).

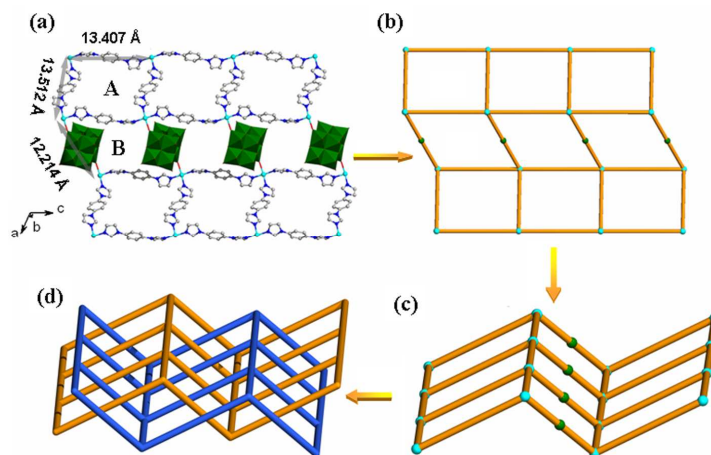


**Fig. 2** (a) View of the 2D network in **1**. (b) Topology of the 2D network in **1**. (c) Topology of the 2D undulated layer. (d) Topology of the (2D → 2D) 2-fold interpenetrating layer.

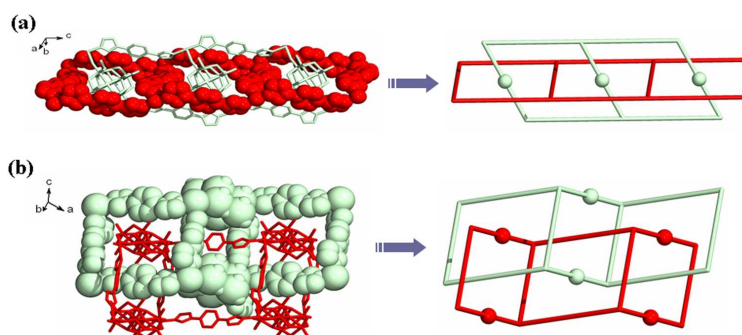


**Fig. 3** Detailed view of the two kinds of interpenetrating motifs in **1**.

### Crystal Structure of compound **2**

X-ray crystal structure analysis reveals that compound **2** consists of one crystallographically independent Cu(I) ion, one bimb ligand, two free protonated bimb ligands and one  $\text{PMo}_{12}\text{O}_{40}^{3-}$  polyanion (abbreviated as  $\text{PMo}_{12}$ ) (Fig. 4). The  $\text{PMo}_{12}$  anion exhibits the well-known  $\alpha$ -Keggin configuration,<sup>20</sup> consisting of central  $\text{PO}_4$  tetrahedron corner-sharing four triad  $\{\text{Mo}_3\text{O}_{13}\}$  clusters. The central four  $\mu_4$ -O atoms are observed to be disordered over eight positions with each oxygen site half-occupied, which is a usual phenomenon for Keggin clusters.<sup>21</sup> If  $\text{Cu}\cdots\text{O}$  interactions (3.032 Å) were considered as weak interactions, the Cu1 ion would be six-coordination in distorted octahedral geometry achieved by two nitrogen atoms

from two bimb ligands and four oxygen atoms from two  $\text{PMo}_{12}$  polyanions. The bond lengths around the Cu ions are 1.867 Å (Cu–N), 2.865 Å (Cu–O).

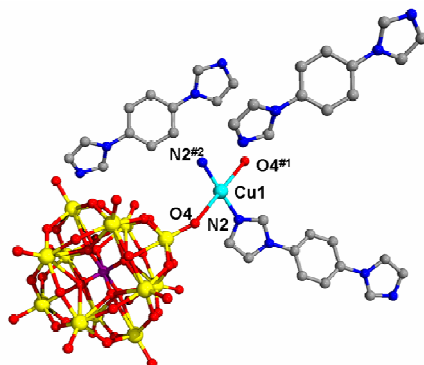


**Fig. 4** Asymmetric unit of compound **2** and the coordination environments around the Cu atoms. (All of the hydrogen atoms are omitted for clarity; Symmetry codes: #1: 1-x, 2-y, 2-z ; #2: 1-x, 1-y, 2-z.)

In **2**, each the  $\text{PMo}_{12}$  polyanion as a double-dentate inorganic ligand links two neighboring Cu-bimb chains to give rise to a 2D ( $4^4$ ) **sql** net with the dimensions of each window *ca.* 14.903 × 13.292 Å (Fig. 5a). Furthermore, as shown in Fig. 5b and 5c, the adjacent **sql** nets are connected together by the hydrogen bonding interactions between  $\text{PMo}_{12}$  polyanions and lattice water molecules to form a highly opened 3D supramolecular framework (typical hydrogen bondings: O1w–H1a $\cdots$ O3 = 3.042 Å, O1w–H1a $\cdots$ O17 = 2.975 Å, O1w–H1b $\cdots$ N4 = 3.22 Å).

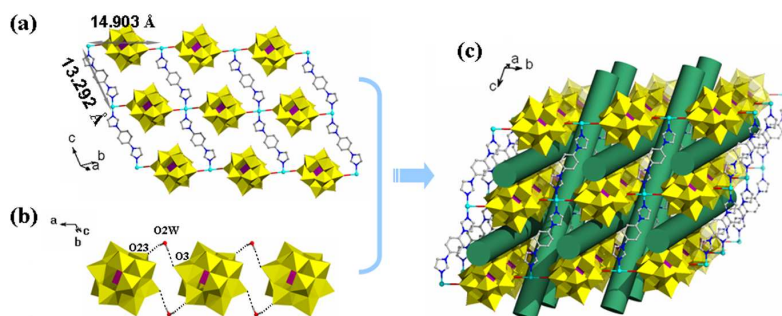


**Fig. 5** View of the Structural motifs in **2**: (a) the 2D grid layer, (b) the hydrogen bonding interactions between  $\text{PMo}_{12}$  polyanions and lattice water molecules, (c) the highly opened 3D supramolecular framework.

### Crystal Structure of compound **3**

Single-crystal X-ray structural analysis reveals that the structure of **3** contains four Cu(I) ions, four bimb ligands and one  $[\text{SiMo}_{12}\text{O}_{40}]^{4-}$  anion (abbreviated as  $\text{SiMo}_{12}$ ) (Fig. 6). The  $\text{SiMo}_{12}$  anion also exhibits the well-known  $\alpha$ -Keggin configuration.<sup>20</sup> There are two crystallographically independent Cu ions in the structure. Both the Cu1 and Cu2 atoms adopt the T-shaped geometry, coordinated by two nitrogen atoms (N1 and N7 for Cu1, N4 and N5 for Cu2) from bimb ligands and one oxygen atom (O1 for Cu1 and O11 for Cu2) from  $\text{SiMo}_{12}$  anion. The Cu–N and Cu–O bond lengths range from 1.864(12) to 1.873(13) Å and 2.561(2) to 2.729(3) Å, respectively.

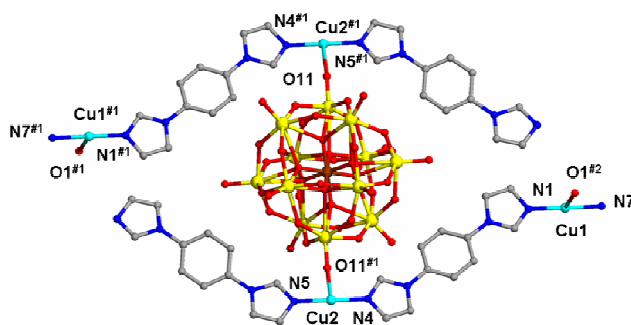


**Fig. 6** Asymmetric unit of compound **3** and the coordination environments around the Cu atoms. (All of the hydrogen atoms are omitted for clarity). (Symmetry codes: #1: 2-x, 2-y, 2-z; #2: -1+x, -1+y, -1+z.)

There are two structural features for **3**. The first one is that there exist the left- and right-handed helical chains running along the [100] direction with an identical screw-pitch of *ca.* 15.381 Å, as shown in Fig. 7a. Another interesting structural feature is the (2D + 2D → 3D) interdigitated architecture that can be described as follows: each  $\text{SiMo}_{12}$  polyanion in **3** acts a di-dentate inorganic ligand to link two neighboring Cu-bimb chains. Consequently, a POM-Cu-bimb rail chain is formed. Further, the adjacent POM-Cu-bimb rail chains are connected together *via* covalent bonds [(Cu1–O1), 2.572 Å] to giving rise to a 2D layer (Fig. S1 and Fig. 7b). From

the topological view, if the Cu1 and Cu2 cations are considered as 3-connected nodes, SiMo<sub>12</sub> anion is considered as 4-connected nodes, respectively. The topology of the 2D layers is the 3,4L90 type.<sup>22</sup> (Fig. 7c). Interestingly, the 2D layer is poly-pendant layer observed from the given direction (Fig. 8, left), in which the bimb ligands as pendants are appended to the two sides of the layer. These concavities of layers are occupied by the protrudent bimb ligands from the adjacent layers to forming a (2D + 2D → 3D) interdigitated architecture (Fig. 8). Complementary intermolecular non-classical hydrogen bondings existing between the two adjacent layers stabilize this structure (All of the hydrogen bondings have been list in Table S1). To the best of our knowledge, the **3** represents the rare example of POM-based inorganic-organic hybrids consisting of both helical and interdigitated motifs up to now.

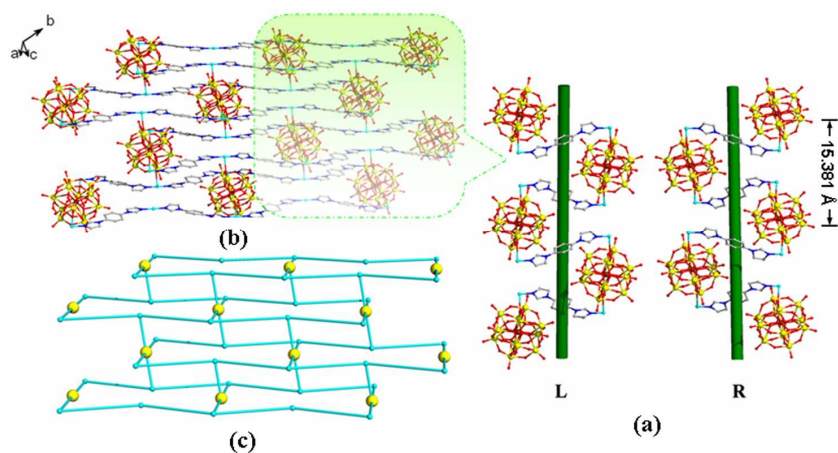


**Fig. 7** View of the Structural motifs in **3**: (a) the left- and right-handed helical chains, (b) the 2D layer and (c) the topology of the 2D layer.

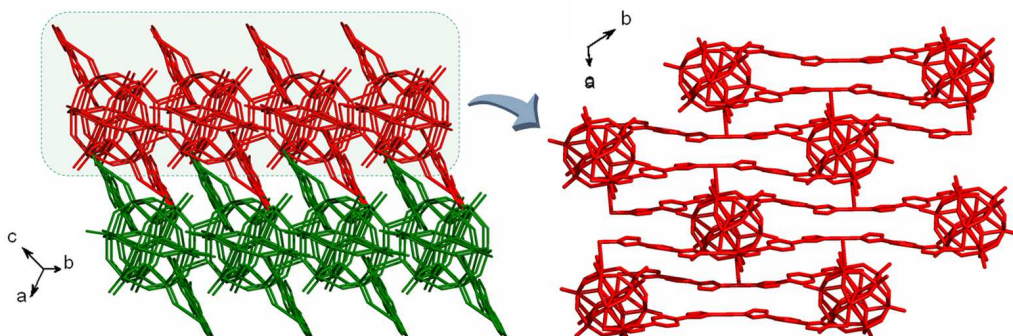
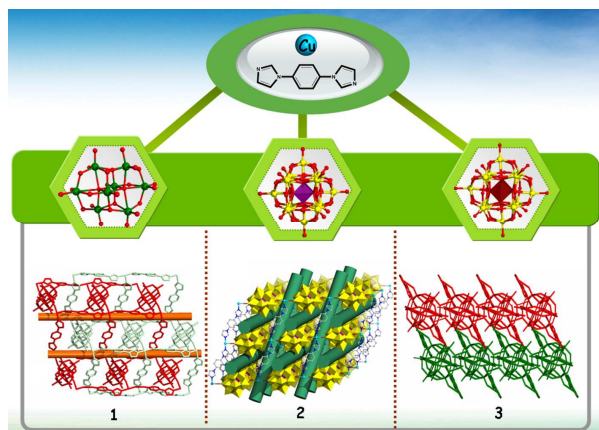


Fig. 8 View of the 2D + 2D  $\rightarrow$  3D interdigitated architecture in **3**.

### Influence of size and charge of different POMs polyoxoanions on structures of the POMs-based inorganic-organic hybrids

The size and charge of different polyoxoanions are known to be two important factors in the modification of the structures of the POM-based inorganic-organic hybrids, however, synergistic reaction of such two effects are seldom considered in the assembly of POM-based hybrids.<sup>23</sup> In this work, the  $\text{Mo}_8$ ,  $\text{PMo}_{12}$  and  $\text{SiMo}_{12}$  POMs clusters are introduced into an identical Cu-bimb reaction system, respectively (**Scheme 1**). Compound **1** shows a (2D  $\rightarrow$  2D) 2-fold interpenetrated structure. When the  $\beta$ - $\text{Mo}_8$  cluster (*ca.* 6.4 Å) was replaced by  $\text{PMo}_{12}$  and  $\text{SiMo}_{12}$  clusters (*ca.* 10.4 Å), respectively, the interpenetrated feature was prevented. It is coincident to the previous investigation that the nanosized POM clusters could break the interpenetrated structures with ease.<sup>24</sup> On the other hand, different charge of the polyoxoanions may also influence the final structures. Generally, from the charge point of view, as the charge density on the surface oxygen atoms of the POM increases, there should appear a significant affinity for the polyoxoanions to highly coordinate to transition metal complex cations.<sup>9a,25</sup> In Keggin group, the  $\text{PMo}_{12}$  and  $\text{SiMo}_{12}$  clusters possess similar size, and obviously different negative charge (-3 for  $\text{PMo}_{12}$  and -4 for  $\text{SiMo}_{12}$

polyoxoanions). Thus, in compound **2**, the  $\text{PMo}_{12}$  cluster as a di-dentate inorganic ligand to link Cu-bimb chain forming an inorganic-organic 2D grid layer. In contrast to compound **2**, in compound **3**, the  $\text{SiMo}_{12}$  cluster acts a tetra-dentate inorganic ligand to link four neighboring Cu-bimb chains finally achieving a  $2\text{D} + 2\text{D} \rightarrow 3\text{D}$  interdigitated architecture. Overall, the informative structures of the three compounds contribute to further understanding of the effect of both size and charge of polyoxoanions on assembly of POM-based hybrids. The further work is still under way in our laboratory.



**Scheme 1.** Summary of the influences of size and charge of the different POM clusters on the structures of compounds **1–3**.

### Analyses of BVS, IR spectra and PXRD

In **1–3**, all Mo atoms are in +VI oxidation state obtained by bond valence sum (BVS) calculations.<sup>26</sup> All copper atoms are in +II oxidation states in **1**, and +I oxidation states in **2** and **3**, respectively, which was confirmed by the BVS calculations, coordination environments, crystal colors and charge balance.

The IR spectra of compounds **1–3** are shown in Fig.S2. The IR spectra exhibit the characteristic peaks at 963, 891, 799 and 688  $\text{cm}^{-1}$  in **1**, 1046, 937, 873 and 780  $\text{cm}^{-1}$  in **2**, 1051, 931, 882 and 774  $\text{cm}^{-1}$  in **3**, which are attributed to  $\nu(\text{Mo}=\text{O}_t)$ ,

$\nu_{as}(\text{Mo}-\text{Ob}-\text{Mo})$  and  $\nu_{as}(\text{Mo}-\text{Oc}-\text{Mo})$  from  $\beta\text{-Mo}_8$  clusters,<sup>15a</sup>  $\nu(\text{P}-\text{O})$ ,  $\nu(\text{Mo}=\text{Ot})$ ,  $\nu_{as}(\text{Mo}-\text{Ob}-\text{Mo})$  and  $\nu_{as}(\text{Mo}-\text{Oc}-\text{Mo})$  from  $\text{PMo}_{12}$  clusters,<sup>27</sup>  $\nu(\text{Si}-\text{O})$ ,  $\nu(\text{Mo}=\text{Ot})$ ,  $\nu_{as}(\text{Mo}-\text{Ob}-\text{Mo})$  and  $\nu_{as}(\text{Mo}-\text{Oc}-\text{Mo})$  from  $\text{SiMo}_{12}$  clusters,<sup>19a</sup> respectively. Additionally, the bands in the region of 1638–1151  $\text{cm}^{-1}$  could be ascribed to the character peaks of bimb ligands in **1–3**.<sup>28</sup>

To indicate the phase purities of compounds **1–3**, the PXRD experiments are carried out. We have refitted by Powder Cell 2.3. As shown in Fig. S3, from the results of fitting, we can see that purity of compound **1** and **2** is good. However, in the PXRD pattern of compound **3**, the diffraction peaks of both simulated and experimental patterns do not match well in some positions may be just ascribed to that the sample has been deposited for long time and might be partly pulverized. And the stability of compound **3** is inferior.

### Photoluminescent properties

Recently, inorganic-organic hybrid coordination polymers, especially comprising aromatic system, have been intensively investigated for attractive fluorescence properties and potential applications as new luminescent materials.<sup>29</sup> In the present work, the photoluminescence properties of compounds **1–3** are investigated in the solid state at room temperature. Meanwhile, in order to understand the nature of the luminescence, the emission spectrum of free bimb ligand was also investigated under similar experimental conditions. As shown in Fig. 9, it can be observed that the free bimb ligand exhibits a intense emission peak at *ca.* 442 nm when excited at 334 nm, which can be assigned to an intraligand ( $\pi\text{-}\pi^*$ ) charge-transfer.<sup>30</sup> However, the

emission peaks of compounds **1–3** are found at *ca.* 467, 517 and 541 nm, respectively, when excitation occurs at 351 nm for **1**, 373 nm for **2** and 387 nm for **3**. Meanwhile, compared to the free bimb ligand, we can observe that the emission spectra of compounds **1–3** are red-shifted. The origin of the emission of compounds **1–3** can be tentatively attributed to ligand-to-metal charge transfer (LMCT).<sup>31</sup> And the significant red-shift compared to the free bimb ligand may be due to the effect of the coordination between ligands and metal ions.<sup>32</sup> Since **1–3** are insoluble in common polar and nonpolar solvents, they may be good candidates for potential solid-state luminescent materials.

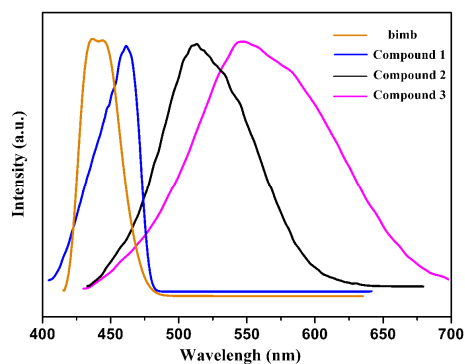


**Fig. 9** The emission spectra of bimb ligand and compounds **1–3** in room temperature.

### The Electrocatalytic Activity of **1–3**-CPEs

The POMs possess the ability of undergoing reversible multi-electron redox processes, which makes them very attractive in chemically-modified electrode and the electrocatalytic study.<sup>33</sup> Due to the title compounds are insoluble in water and common organic solvents. Thus, the bulk-modified carbon paste electrode (CPE) becomes the optimal choice to study the electrochemical properties, which is inexpensive, easy to prepare and handle.<sup>34</sup>

The cyclic voltammograms for **1–3**-CPEs in the 1 M H<sub>2</sub>SO<sub>4</sub> aqueous solution at different scan rates are presented in Fig. 10. It can be seen clearly that two reversible redox peaks (I-I', II-II') appear in the potential range from +0.65 to -0.1 V for **1**-CPE. The mean peak potentials  $E_{1/2} = (E_{pa} + E_{pc})/2$  are +0.38 (I-I') and +0.17 V (II-II') (scan rate: 50 mV·s<sup>-1</sup>), which can be ascribed to redox of Mo<sub>8</sub> polyanions.<sup>35</sup> In the same potential range for **2**- and **3**-CPEs, it can be seen that there are three pairs of reversible redox peaks with the mean peak potentials  $E_{1/2} = (E_{pa} + E_{pc})/2$  are +0.39 V (I-I'), +0.22 V (II-II'), -0.032 V (III-III'), and +0.42 V (I-I'), +0.25 V (II-II'), -0.028 V (III-III') which can be ascribed to redox of PMo<sub>12</sub> and SiMo<sub>12</sub> polyanions, respectively.<sup>27,19a</sup> When the scan rates increased, the cathodic peak currents and the corresponding anodic peak currents increased simultaneously, which are proportional to scan rates (Fig. S4), suggesting that the redox processes of **1–3**-CPEs is surface-controlled and the exchanging rate of electrons is fast.<sup>36</sup>

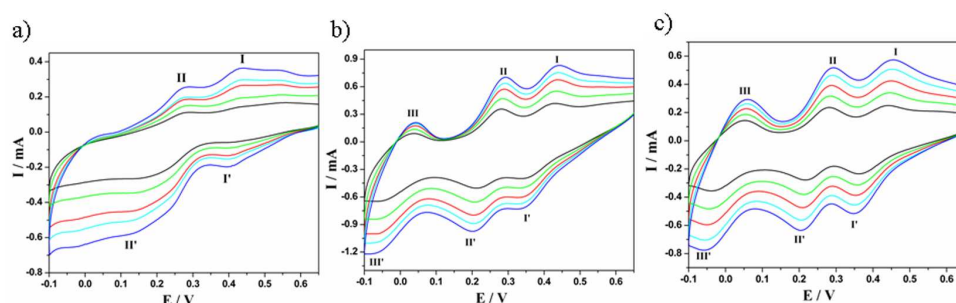


**Fig. 10** (a) Cyclic voltammograms for **1**-CPE; (b) **2**-CPE; (c) **3**-CPE in 1 M H<sub>2</sub>SO<sub>4</sub> aqueous solution at different scan rates (from inner to outer: 50, 75, 100, 125 and 150 mV s<sup>-1</sup>), respectively.

The electrocatalytic properties of **1–3**-CPEs have also been investigated toward reduction iodated (IO<sub>3</sub><sup>-</sup>) in 1 M H<sub>2</sub>SO<sub>4</sub> aqueous solution. The results show that the **1**-, **2**- and **3**-CPEs have electrocatalytic activities for iodated. As shown in Fig. S5, with addition of iodated, all the reduction peak currents increase gradually while the

corresponding oxidation peak currents decrease suggesting that the reduction of iodated is mediated by the reduced species of  $\text{Mo}_8$  polyanions in **1**,  $\text{PMo}_{12}$  polyanions in **2** and  $\text{SiMo}_{12}$  polyanions in **3**. The dependence curves of reduction peak currents  $I$  on concentration of iodated are presented in Fig. S6. As shown in Fig. S6, the nearly equal current steps for each addition of  $\text{IO}_3^-$  also demonstrate stable and efficient electrocatalytic activities of the CPEs.

To compared the electrocatalytic activity of **1**-, **2**- and **3**-CPEs for iodated, the CATs (catalytic efficiencies) of **1**-, **2**- and **3**-CPEs can be calculated by using CAT formula.<sup>37</sup> As shown in Fig. 11, the CAT of **1**-, **2**- and **3**-CPEs towards 20 mM  $\text{IO}_3^-$ , were calculated to be 291 %, 43 % and 92 %, respectively. The **1**-CPE has the best electrocatalytic efficiency towards the reduction of iodated, which suggests that compound **1** has potential applications in detection of iodated. Additionally, the stability experiments for **1**–**3**-CPEs have been investigated by cyclic voltammetry scanning for 40 cycles in 1 M  $\text{H}_2\text{SO}_4$  solution, respectively. As shown in Fig. S7, it can be seen that the electrode exhibits almost no loss in the current signal after 40 cycles, which suggests that the catalyst of **1**–**3**-CPEs have high stabilities.

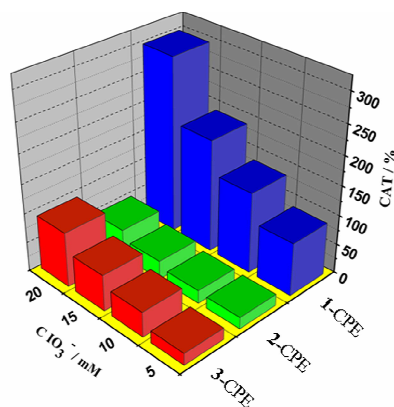


**Fig. 11** Chart of the CATs (catalytic efficiencies) vs concentration of the iodated ( $\text{IO}_3^-$ ).

## Conclusions

In summary, three new polyoxomolybdate-based inorganic-organic hybrids have been synthesized by introducing different polyoxomolybdates into the Cu-bimb system, to investigate influence of the size and charge of different polyoxoanions in the assembly processes. The informative structures of the title compounds illustrates that size of the polyoxometalate clusters can play a key role on controlling the interpenetration of frameworks, but also further confirms that the charge of polyoxoanions is another important factor in the assembly processes. To some extent, this work may provide a useful example for step by step understanding the influences of polyoxometalate clusters on the assembly processes in hydrothermal conditions and shows the perspective for synthesis of new polyoxometalate-based hybrid materials through reasonable selection of the polyoxometalate clusters.

## Acknowledgments

This work was financially supported by the NSF of China (21371041), youth scholar backbone supporting plan project for general universities of Heilongjiang Province (1254G020), and the science and technology innovation foundation of Harbin (2014RFXXJ076, 2013RFQXJ144).

## References

- (1) (a) S. Kitagawa, R. Kitaura and S. Noro, *Angew. Chem., Int. Ed.*, 2004, **43**, 2334; (b) H. K. Chae, D. Y. Siberio-Pérez, J. Kim, Y. Go, M. Eddaoudi, A. J. Matzger, M. O’Keeffe and O. M. Yaghi, *Nature*, 2004, **427**, 523; (c) M. Eddaoudi, D. B.

- Moler, H. L. Li, B. L. Chen, T. M. Reineke, M. O’Keeffe and O. M. Yaghi, *Acc. Chem. Res.*, 2001, **34**, 319; (d) S. R. Battan and K. S. Murray, *Coord. Chem. Rev.*, 2003, **246**, 103; (e) A. R. Millward and O. M. Yaghi, *J. Am. Chem. Soc.*, 2005, **127**, 17998; (f) M. Kondo, T. Yoshitomi, K. Seki, H. Matsuzaka and S. Kitagawa, *Angew. Chem., Int. Ed.*, 1997, **36**, 1725; (g) N. L. Rosi, J. Eckert, M. Eddaoudi, D. T. Vodak, J. Kim, M. O’Keeffe and O. M. Yaghi, *Science*, 2003, **300**, 1127; (h) T. K. Holman, *Angew. Chem., Int. Ed.*, 2011, **50**, 1228.
- (2) (a) O. M. Yaghi, M. O’Keeffe, N. W. Ockwig, H. K. Chae, M. Eddaoudi and J. Kim, *Nature*, 2003, **423**, 705; (b) J. L. C. Rowsell, E. C. Spencer, J. Eckert, J. A. K. Howard and O. M. Yaghi, *Science*, 2005, **309**, 1350; (c) C. G. Bezzu, M. Helliwell, J. E. Warren, D. R. Allan and N. B. McKeown, *Science*, 2010, **327**, 1627; (d) L. Carlucci, G. Ciani and D. M. Proserpio, *Coord. Chem. Rev.*, 2003, **246**, 247; (e) Q. Li, C. H. Sue, S. Basu, A. K. Shveyd, W. Zhang, G. Barin, L. Fang, A. A. Sarjeant, J. F. Stoddart and O. M. Yaghi, *Angew. Chem., Int. Ed.*, 2010, **49**, 6751; (f) W. H. Fang, L. Cheng, L. Huang and G. Y. Yang, *Inorg. Chem.*, 2013, **52**, 6.
- (3) (a) P. J. Hagrman, D. Hagrman and J. Zubieta, *Angew. Chem., Int. Ed.*, 1999, **38**, 2638; (b) A. Müller, M. T. Pope, F. Peters and D. Gatteschi, *Chem. Rev.*, 1998, **98**, 239; (c) B. K. Won, T. Voitl, G. J. RodríguezRivera and J. A. Dumesic, *Science*, 2004, **305**, 1280; (d) B. Z. Lin and S. X. Liu, *Chem. Commun.*, 2002, 2126; (e) T. McGlone, J. Thiel, C. Streb, D. L. Long and L. Cronin, *Chem. Commun.*, 2012, **48**, 359; (f) S. Uchida, R. Eguchi and N. Mizuno, *Angew. Chem., Int. Ed.*, 2010, **49**, 9930; (g) X. K. Fang, P. Kögerler, L. Isaacs, S. Uchida and N.

- Mizuno, *J. Am. Chem. Soc.*, 2009, **131**, 432; (h) A. Dolbecq, E. Dumas, C. R. Mayer and P. Mialane, *Chem. Rev.*, 2010, **110**, 6009; (i) D. Y. Du, L. K. Yan, Z. M. Su, S. L. Li, Y. Q. Lan and E. B. Wang, *Coord. Chem. Rev.*, 2013, **257**, 702; (j) D. Y. Du, J. S. Qin, S. L. Li, Z. M. Su and Y. Q. Lan, *Chem Soc Rev.*, 2014, **43**, 4615.
- (4) A. Dolbecq, E. Dumas, C. R. Mayer and P. Mialane, *Chem. Rev.*, 2010, **110**, 6009.
- (5) (a) Q. X. Han, C. He, M. Zhao, B. Qi, J. Y. Niu and C. Y. Duan, *J. Am. Chem. Soc.*, 2013, **135**, 10186; (b) J. Song, Z. Luo, D. K. Britt, H. Furukawa, O. M. Yaghi, K. I Hardcastle and C. L. Hill, *J. Am. Chem. Soc.*, 2011, **133**, 16839; (c) F. J. Ma, S. X. Liu, C. Y. Sun, D. D. Liang, G. J. Ren, F. Wei, Y. G. Chen and Z. M. Su, *J. Am. Chem. Soc.*, 2011, **133**, 4178; (d) B. Nohra, H. E. Moll, L. M. R. Albelo, P. Mialane, J. Marrot, C. Mellot-Draznieks, M. O 'Keeffe, R. N. Biboum, J. Lemaire, B. Keita, L. Nadjjo and A. Dolbecq, *J. Am. Chem. Soc.*, 2011, **133**, 13363.
- (6) (a) A. X. Tian, J. Ying, J. Peng, J. Q. Sha, Z. G. Han, J. F. Ma, Z. M. Su, N. H. Hu and H. Q. Jia, *Inorg. Chem.*, 2008, **47**, 3274; (b) A. X. Tian, J. Ying, J. Peng, J. Q. Sha, H. J. Pang, P. P. Zhang, Y. Chen, M. Zhu and Z. M. Su, *Cryst. Growth Des.*, 2008, **8**, 3717.
- (7) (a) T. M. Anderson, W. A. Neiwert, K. I. Hardcastle and C. L. Hill, *Inorg. Chem.*, 2004, **43**, 7353; (b) C. Zhang, R. C. Howell, K. B. Scotland, F. G. Perez, L. Todaro and L. C. Francesconi, *Inorg. Chem.*, 2004, **43**, 7691.
- (8) (a) E. Burkholder, V. Golub, C. J. O'Connorr and J. Zubietta, *Inorg. Chem.*, 2004, **43**, 7014; (b) Z. Y. Shi, J. Peng, C. J. Gómez-García, S. Benmansour and X. J.

- Gu, *J. Solid State Chem.*, 2006, **179**, 253; (c) Y. Q. Lan, S. L. Li, K. Z. Shao, X. L. Wang and Z. M. Su, *Dalton Trans.*, 2008, 3824.
- (9) (a) S. B. Li, W. Zhu, H. Y. Ma, H. J. Pang, H. Liu and T. T. Yu, *RSC. Advances.*, 2013, **3**, 9770; (b) S. B. Li, H. Y. Ma, H. J. Pang, Z. F. Zhang, Y. Yu, H. Liu and T. T. Yu, *CrystEngComm.*, 2014, **16**, 2045; (c) S. B. Li, W. L. Sun, K. Wang, H. Y. Ma, H. J. Pang, H. Liu and J. X. Zhang, *Inorg. Chem.*, 2014, **53**, 4541; (d) D. Wu, K. Wang, H. R. Ma, H. J. Pang, T. T. Yu, Z. F. Zhang, S. B. Li and H. Liu, *Solid State Sci.*, 2014, **35**, 39.
- (10) (a) W. G. Klemperer, T. A. Marquart and O. M. Yaghi, *Angew. Chem., Int. Ed.*, 1992, **31**, 49. (b) W. G. Klemperer, T. A. Marquart and O. M. Yaghi, *Angew. Chem. Int. Ed.*, 1992, **104**, 51; (c) V. W. Day, W. G. Klemperer and O. M. Yaghi, *J. Am. Chem. Soc.*, 1989, **111**, 5959; (d) G. K. Johnson and E. O. Schlemper, *J. Am. Chem. Soc.*, 1978, **100**, 3645; (e) L. Chen, F. L. Jiang, Z. Z. Lin, Y. F. Zhou, C. Y. Yue and M. C. Hong, *J. Am. Chem. Soc.*, 2005, **127**, 8588; (f) M. I. Khan and J. Zubieta, *Angew. Chem., Int. Ed.*, 1994, **33**, 760.
- (11) (a) X. L. Hao, Y. Y. Ma, Y. H. Wang, L. Y. Xu, F. C. Liu, M. M. Zhang and Y. G. Li, *Chem. Asian J.*, 2014, **9**, 819; (b) M. T. Li, J. Q. Sha, X. M. Zong, J. W. Sun, P. F. Yan, L. Li and X. N. Yang, *Cryst. Growth Des.*, 2014, **14**, 2794; (c) X. L. Wang, D. Zhao, A. X. Tian and J. Ying, *Dalton Trans.*, 2014, **43**, 5211.
- (12) Sheldrick, G. M. *SADABS 2.05*; University of Göttingen: Göttingen, Germany.
- (13) *SHELXTL 6.10*; Bruker Analytical Instrumentation: Madison, WI, 2000.
- (14) Dolomanov, O. V.; Blake, A. J.; Champness, N. R.; Schröder, M. J. *Appl. Crystallogr.*, 2003, **36**, 1283.

- (15) (a) C. J. Zhang, H. J. Pang, Q. Tang, H. Y. Wang and Y. G. Chen, *New J. Chem.*, 2011, **35**, 190; (b) C. J. Zhang, H. J. Pang, Q. Tang, H. Y. Wang and Y. G. Chen, *Dalton Trans.*, 2010, **39**, 7993; (c) S. L. Li, Y. Q. Lan, J. F. Ma, J. Yang, X. H. Wang and Z. M. Su, *Inorg. Chem.*, 2007, **46**, 8283.
- (16) J. Q. Sha, J. Peng, Y. Zhang, H. J. Pang, A. X. Tian, P. P. Zhang and H. Liu, *Cryst Growth Des.*, 2009, **9**, 1708.
- (17) L. Carlucci, G. Ciani, D. M. Proserpio, T. G. Mitina and V. A. Blatov, *Chem. Rev.*, 2014, **114**, 7557.
- (18) W. W. He, S. L. Li, H. Y. Zang, G. S. Yang, S. R. Zhang, Z. M. Su and Y. Q. La, *Coord. Chem. Rev.*, 2014, 279, 141.
- (19) (a) B. X. Dong and Q. Xu, *Cryst Growth Des.*, 2009, **9**, 2776; (b) B. X. Dong and Q. Xu, *Inorg. Chem.*, 2009, **48**, 5861; (c) H. Y. Liu, H. Wu, J. F. Ma, Y. Y. Liu, J. Yang and J. C. Ma, *Dalton Trans.*, 2011, **40**, 602.
- (20) F. Keggin, *Nature*, 1933, **131**, 908.
- (21) (a) H. T. Evans and M. T. Pope, *Inorg. Chem.*, 1984, **23**, 501; (b) H. J. Pang, J. Peng, C. J. Zhang, Y. G. Li, P. P. Zhang, H. Y. Ma and Z. M. Su, *Chem. Commun.*, 2010, **46**, 5097.
- (22) T. G. Mitina and V. A. Blatov, *Cryst Growth Des.*, 2013, **13**, 1655.
- (23) (a) J. Q. Sha, J. Peng, A. X. Tian, H. S. Liu, J. Chen, P. P. Zhang and Z. M. Su, *Cryst. Growth Des.*, 2007, **7**, 2535; (b) Y. N. Chi, F. Y. Cui, Z. G. Lin, Y. Xu, X. Y. Ma, P. P. Shen, K. L. Huang and C. W. Hu, *J. Solid State Chem.*, 2013, **199**, 230; (c) Y. Yu, H. Y. Ma, H. J. Pang, L. Zhang, S. B. Li, C. Y. Zhao and Z. Z. Zhang, *RSC Adv.*, 2014, **4**, 61210.
- (24) (a) B. X. Dong, J. Peng, C. J. Gómez-García, S. Benmansour, H. Q. Jia and N. H.

- Hu, *Inorg. Chem.*, 2008, **46**, 5933; (b) H. J. Pang, H. Y. Ma, J. Peng, C. J. Zhang, P. P. Zhang, Z. M. Su, *CrystEng Comm.*, 2011, **13**, 7079.
- (25) C. J. Zhang, H. J. Pang, Q. Tang, Y. G. Chen, *Dalton Trans.*, 2012, **41**, 9365.
- (26) I. D. Brown and D. Altermatt, *Acta Crystallogr. Sect. B: Struct. Sci.*, 1985, **41**, 244.
- (27) X. L. Wang, Y. F. Bi, B. K. Chen, H. Y. Lin and G. C. Liu, *Inorg. Chem.*, 2008, **47**, 2442.
- (28) H. Y. Zang, Y. Q. Lan, S. L. Li, G. S. Yang, K. Z. Shao, X. L. Wang, L. K. Yan and Z. M. Su, *Dalton Trans.*, 2011, **40**, 3176.
- (29) (a) Y. Bai, G. Q. Zhang, D. B. Dang, P. T. Ma, H. Gao and J. Y. Niu, *CrystEngComm.*, 2011, **13**, 4181; (b) S. Igawa, M. Hashimoto, I. Kawata, M. Hoshino and M. Osawa, *Inorg. Chem.*, 2012, **51**, 5805.
- (30) (a) Y. Gong, T. Wu and J. Lin, *CrystEngComm.*, 2012, **14**, 3727; (b) H. Y. Bai, J. F. Ma, J. Yang, L. P. Zhang, J. C. Ma and Y. Y. Liu, *Cryst. Growth Des.*, 2010, **10**, 1946.
- (31) (a) X. He, J. Zhang, X. Y. Wu and C. Z. Lu, *Inorg. Chim. Acta.*, 2010, **363**, 1727; (b) W. Li, H. P. Jia, Z. F. Ju and J. Zhang, *Cryst. Growth Des.*, 2006, **6**, 2136; (c) Z. Su, J. Fan, M. Chen, T. A. Okamura and W. Y. Sun, *Cryst. Growth Des.*, 2011, **11**, 1159.
- (32) H. Y. Zang, D. Y. Du, S. L. Li, Y. Q. Lan, G. S. Yang and L. K. Yan, *J. Solid State Chem.*, 2011, **184**, 1141.
- (33) X. D. Xi, G. Wang, B.F. Liu and S.J. Dong, *Electrochim. Acta.*, 1995, **40**, 1025.
- (34) Z. G. Han, Y. L. Zhao, J. Peng, Y. H. Feng, J. N. Yin and Q. Liu, *Electroanalysis.*, 2005, **17**, 1097.

- (35) (a) H. Jin, Y. F. Qi, E. B. Wang, Y. G. Li, C. Qin, X. L. Wang and S. Chang, *Eur. J. Inorg. Chem.*, 2006, 4541; (b) C. Qin, X. L. Wang, Y. F. Qi, E. B. Wang, C. W. Hu and L. Xu, *J. Solid State Chem.*, 2004, **177**, 3263.
- (36) X. L. Wang, Q. Gao, A. X. Tian, H. L. Hu and G. C. Liu, *J. Solid State Chem.*, 2012, **187**, 219.
- (37) B. Keita, A. Belhouari, L. Nadjo and R. Contant, *J. Electroanal. Chem.*, 1995, **381**, 243.